RSC Advances

PAPER

View Article Online
View Journal | View Issue

Cite this: *RSC Adv.*, 2021, **11**, 25664

Study of physical properties of a ferrimagnetic spinel $Cu_{1.5}Mn_{1.5}O_4$: spin dynamics, magnetocaloric effect and critical behavior

Abir Hadded, *[a] Jalel Massoudi, *[a] Sirine Gharbi,[a] Essebti Dhahri,[a] A. Tozri[b] and Mohamed R. Berber*[c]

The present work reports a detailed study of the spin dynamics, magnetocaloric effect and critical behaviour near the magnetic phase transition temperature, of a ferrimagnetic spinel $Cu_{1.5}Mn_{1.5}O_4$. The dynamic magnetic properties investigated using frequency-dependent ac magnetic susceptibility fitted using different phenomenological models such as Neel–Arrhenius, Vogel–Fulcher and power law, strongly indicate the presence of a cluster-glass-like behavior of $Cu_{1.5}Mn_{1.5}O_4$ at 40 K. The magnetization data have revealed that our compound displays an occurrence of second-order paramagnetic (PM) to ferrimagnetic (FIM) phase transition at the Curie temperature $T_C = 80$ K as the temperature decrease. In addition, the magnetic entropy change (ΔS_M) was calculated using two different methods: Maxwell relations and Landau theory. An acceptable agreement was found between both sets of data, which proves the importance of both electron interaction and magnetoelastic coupling in the magnetocaloric effect (MCE) properties of $Cu_{1.5}Mn_{1.5}O_4$. The relative cooling power (RCP) reaches 180.13 (J kg^{-1}) for an applied field at 5 T, making our compound an effective candidate for magnetic refrigeration applications. The critical exponents β, γ and δ as well as transition temperature T_C were extracted from various techniques indicating that the magnetic interaction in our sample follows the 3D-Ising model. The validity of the critical exponents is confirmed by applying the Windom scaling hypothesis.

Received 12th May 2021
Accepted 13th July 2021

DOI: 10.1039/d1ra03732c

rsc.li/rsc-advances

1. Introduction

There is a category of double oxides of general formula AB_2O_4 which includes two types of arrangements. In the first possible distribution, known as normal spinel, the A^{2+} cations occupy the tetrahedral interstitial sites and the B^{3+} cations occupy the octahedral sites. This distribution is indicated as $(A^{2+})[B_2^{3+}]O_4$ where the parentheses designate the tetrahedral, and the brackets, the octahedral positions. A second possible arrangement, $(B^{3+})[A^{2+}B^{3+}]O_4$ known as perfectly inverse spinel, is characterized by B cations occupying all of the tetrahedral and half of the octahedral sites, while the other species (A) occupies the remaining (half of the) octahedral sites. Prototypical examples of normal and inverse spinels are $MgAl_2O_4$ (space group $Fd\bar{3}m$) and $MgGa_2O_4$ (space group $P4_122$), respectively.[1,2] Otherwise, there are many possible intermediate distributions represented by the formula $(A_{1-i}^{2+}B_i^{3+})[A_i^{2+}B_{2-i}^{3+}]O_4$, where i denotes the inversion degree. Magnetic spinel oxides have been extensively investigated owing to their physical properties.[3] They exhibit various magnetic, dielectric, and optical properties, according to their structures, compositions and cation distributions.[4–6] Several cations can be placed in tetrahedral A and octahedral B sites to adjust the magnetic properties. They can present paramagnetic, ferrimagnetic, spin glass and antiferromagnetic behavior, depending on A and B site cations.[7,8] Besides, nonmagnetic ions occupying the A or B sites will lead to magnetic frustration, so that one new magnetic phase will be detected, such as semi-spin-glass (SSG), re-entrant spin-glass (RSG) and spin-glass (SG).[9–11] The existence of the SG comportment is closely associated with the magnetic frustration,[12,13] concluding therefore, that system with lowest energy tend not to be stable.[14] In recent years, magnetic materials have attracted increasing interest among a wide range of researchers whose concern has been grown with the investigation of the potential use in various applications, including but not limited magnetocaloric refrigeration,[15] magnetically guided drug delivery,[16] magnetic resonance imaging (MRI) enhancement,[17] ferrofluid technology,[18] and high-density information storage.[19] Fe_3O_4 or magnetite, is the most-studied spinel ferrite. Recently, the magnetotransport of magnetite has attracted much attention due to the discovery of giant magnetoresistance (GMR) effective in this material.[20] Raman spectroscopy has proven effective in studying the elementary excitation of material. A physical explanation of the enhanced electron–electron correlation in the presence of a magnetic field is proposed to be responsible for the GMR mechanical in magnetite material.[21] The dynamics of

[a]*Laboratoire de Physique Appliquée, Faculté des Sciences, Université de Sfax, 3000, Tunisia. E-mail: abir.hadded1994@gmail.com; jalel.massoudi@gmail.com*
[b]*Physics Department, College of Science, Jouf University, Sakaka 2014, Saudi Arabia*
[c]*Chemistry Department, College of Science, Jouf University, Sakaka 2014, Saudi Arabia*

magnetic superparamagnetic particles have been a subject of intense study in fundamental physics research.[22–24] Cluster glass are kind of spin glasses. In CG groups of spins are locally ordered creating small domains which interact between each other similar to single spins in simple spin glass. To distinguish simple SG from CG few points are considered: relative shift per frequency decade of freezing temperature is much lower for CG,[25,26] the temperature where ZFC magnetic susceptibility reach maximum (T_{max}) and a value of magnetic susceptibility maximum (χ_{max}) strongly depend on applied magnetic field,[27] the monotonic increase of FC ($\chi(T)$ for field-cooling) line with decreasing temperature is characteristic for CG compounds,[27,28] whereas, in simple spin-glass small cusps in the FC behaviour is often visible. The study of magnetic spin behavior is still very limited, which needs to be explored. To our knowledge, until now, no report was available which deals with the relaxation studies of a $Cu_{1.5}Mn_{1.5}O_4$ in a single nanostructure. Many researches have been devoted to the critical behavior of magnetic materials with the aim of reporting a detailed description of the interactions between the spins. Theoretical researches demonstrate that magnetic behavior was described by short-range interactions.[29,30] Other researchers have identified that critical exponents are in accord with a long-range exchange interaction model.[31] The study of the critical properties has been reported for the first time in the mean field theory.[32] But currently, there are 4 different theoretical models that can describe the magnetic interactions. The mean field model ($\beta = 0.5$, $\gamma = 1$ and $\delta = 3$) describes long-range exchange interactions neglecting critical fluctuations in the vicinity of the Curie temperature T_C.[31] The 3D Heisenberg model ($\beta = 0.365$, $\gamma = 1.336$ and $\delta = 4.80$) describes short-range exchange interactions at the occurrence of spin fluctuations near T_C.[31] In the 3D Ising model ($\beta = 0.325$, $\gamma = 1.240$ and $\delta = 4.82$), the spins interact with their neighbors that are usually arranged in a lattice, and their magnetic dipolar moments that can be in one of the two states ± 1.[31] Finally, the tricritical mean field model ($\beta = 0.25$, $\gamma = 1$ and $\delta = 5$) proposes that the sample's composition should be close to a tri-critical point in the phase diagram of the used material.[31] Recently, there has been a swell of interest in materials containing copper and manganese oxides with spinel structures owing to their interesting magnetic properties.[33–35] $Cu_{1.5}Mn_{1.5}O_4$ is a typical example, crystallizing with a spinel structure, with cationic distributions $[Cu^+]_A[Cu_{0.5}{}^{2+}Mn_{1.5}{}^{4+}]_BO$ Cu^+ of $[Ar]3d^{10}$ electronic configuration occupies the tetrahedral site A while Cu^{2+} ($[Ar]3d^9$) and Mn^{4+} ($[Ar]3d^3$) occupy the octahedral site.[36–38] For the $Cu_{1.5}Mn_{1.5}O_4$ system, both the valance states of Cu ions (Cu^{1+}/Cu^{2+}) and Mn ions (Mn^{4+}) and their site occupancies at the tetrahedral (A site) and octahedral (B site) sites have large flexibilities and hence the affecting magnetic properties, it can be justified by superexchange coupling between the sublattices, and the fact that the local ferrimagnetic order of Mn^{4+} ions on B sites can be disturbed by Cu^{2+} on the same sites.

The present paper reports that ac susceptibility shows the cluster glass behavior of $Cu_{1.5}Mn_{1.5}O_4$ compound. We identified the magnetic properties of ferrimagnetic spinel $Cu_{1.5}Mn_{1.5}O_4$. The study of magnetocaloric properties has a twofold objective. Firstly, from a fundamental point of view, our sample offers an opportunity to investigate the MCE associated with a magnetic transition. Secondly, from an application point of view, it's considered as a good candidate for the cooling system based on magnetic refrigeration. Furthermore, we will determine the critical exponents β, γ and δ in order to identify the model describing the nature of the magnetic interaction in our sample. To date, no research papers have been devoted to study these properties associated with such compound.

2. Experimental techniques

$Cu_{1.5}Mn_{1.5}O_4$ compound were synthesized by the sol–gel method described in our previous study.[39] Low-field ac-susceptibility measurements were made at various frequencies in a temperature range of 20 to 122 K. Magnetic measurements were recorded using a SQUID magnetometer. The magnetization measurements were carried out according to the zero field cooling (ZFC) and field cooling (FC) protocols under 500 Oe and in a temperature range of 20 to 122 K. The isothermal magnetization $M(T, H)$ was recorded for different temperatures under a magnetic field up to 5 T.

3. Results and discussions

3.1 Magnetic measurements

Fig. 1a illustrates the variation of the magnetization as a function of temperature for $Cu_{1.5}Mn_{1.5}O_4$ the magnetic measurements of which were carried out under 500 Oe according to the zero field cooling (ZFC) and field cooling (FC) protocols. The magnetization presents two different regions as a function of temperature. At high temperature, the two curves correspond to superimpose and reversible common part. The other at low temperature, in which a maximum in the ZFC magnetization can be observed below the magnetic irreversibility temperature (T_{irr}). The magnetic behavior is irreversible revealing the magnetic anisotropy.[40] For the $Cu_{1.5}Mn_{1.5}O_4$ compound, the obvious bifurcation between the FC and ZFC M–T curves occurs in the irreversible temperature (T_{irr}). This phenomenon, known as low temperature glassy magnetic state, could be a spin glass,[41] a canonical spin glass[41,42] or a cluster glass.[43] The magnetic transition temperature ($T_C = 80$ K) has been determined using the magnetization derivative dM/dT curve (inset Fig. 1a). A similar behavior was observed in the case of $CuMn_2O_4$ system.[35,44,45]

Aiming to achieve a better understanding of the magnetic behavior of $Cu_{1.5}Mn_{1.5}O_4$ we have plotted the variation of the inverse of magnetic susceptibility as a function of the temperature in the PM region. Fig. 1b display a parabolical variation above 80 K, suggesting the existence of ferrimagnetic behavior ($T_C = 80$ K and $\theta_{CW} = -72$ K) due to the anti-parallel order of the magnetic moments of the nearest neighbor of unequal magnitude.[46] This result is significantly different from the reported results of $Cu_{1.5}Mn_{1.5}O_4$.[47] The synthesized system, using the one-step self-assembly pathway, exhibit ferromagnetic transition phase at room temperature. Therefore the preparation method and the annealing temperature affecting magnetic phase transition.

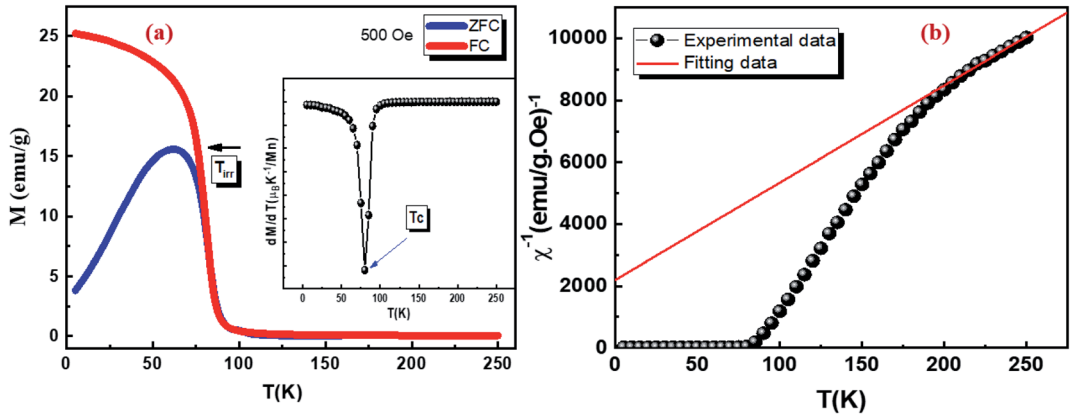

Fig. 1 Magnetization of $Cu_{1.5}Mn_{1.5}O_4$ after zero-field cooling (ZFC) and during field cooling (FC) acquired under a field of 0.05 T, the inset shows the dM/dT curve as a function of temperature (a). Temperature dependence of the inverse magnetic susceptibility $\chi^{-1}(T)$, the solid line is the linear fit to the susceptibility data according to Curie–Weiss law in paramagnetic regime (b).

Table 1 Comparison of magnetic parameters of our sample with several copper manganese mixed oxide spinel

Material	T_C (K)	C (emu K mol^{-1})	θ_{CW} (K)	μ_{eff}^{exp} (μ_B)	Ref.
$Cu_{1.5}Mn_{1.5}O_4$	80	3.198	−72	5.058	This work
$CuMn_2O_4$ (tetragonal)	76	2.43	−76	4.37	35
$CuGaMnO_4$	21	3	−16	4.8	50
$CuMn_2O_4$ (cubic)	73	2.027	−77.4	—	34

The inverse magnetic susceptibility curve above 80 K has been fitted by the Curie–Weiss law:[48]

$$\chi^{-1}(T) = \frac{T - \theta_{CW}}{C} \quad (1)$$

whereby, θ_{CW} is the Curie–Weiss paramagnetic temperature and C is the Curie constant.

The obtained fitted parameters values for $Cu_{1.5}Mn_{1.5}O_4$ are $\theta_{CW} = -72$ K and $C = 3.198$. The obtained value of θ_{CW} is negative, confirm the FIM character of our compound.

The experimental effective moments can be calculated (in unit of Bohr magneton μ_B) from the Curie constant using the following relation:[49]

$$C = \frac{N_A}{3K_B{\mu_B}^3}{\mu_{eff}}^2{\mu_B}^2 \quad (2)$$

whereby $N_A = 6.0231 \times 10^{23}$ mol^{-1} is Avogadro number.

In Gaussian CGS units $\mu_B = 0.9274 \times 10^{-21}$ is the Bohr magneton and $K_B = 1.38016 \times 10^{-16}$ erg. K is Boltzmann constant.

In this case μ_{eff}^{exp} is written:

$$\mu_{eff}^{exp} = \sqrt{\frac{3K_BC}{N_A{\mu_B}^2}}\mu_B = \sqrt{8\cdot C}\mu_B \quad (3)$$

The obtained values of μ_{eff}^{exp} is found to be equal to 5.058 μ_B.

From the cationic distributions $[Cu^+]_A[{Cu_{0.5}}^{2+}{Mn_{1.5}}^{4+}]_BO_4$, the theoretical effective magnetic moment is given by:

$$\mu_{eff}^{the} = \sqrt{0.5 \times {\mu_{eff}}^2(Cu^{2+}) + 1.5 \times {\mu_{eff}}^2(Mn^{4+})} \quad (4)$$

The value of μ_{eff}^{the} is 4.899 μ_B. This μ_{eff}^{the} is very close to our μ_{eff}^{exp}.

The obtained values of T_C, C, θ_{CW} and μ_{eff}^{exp} for our sample are compared with different copper manganese, mixed oxide spinel[34,35,50] listed in Table 1.

3.2 Ac susceptibility

The present research paper seeks to gain a better comprehension of the magnetic order state and the dynamic behavior in our sample. We, therefore, commenced by carrying out ac susceptibility measurements under low magnetic fields ranging from 5 Hz to 950 Hz. Fig. 2a exhibits the real part (χ') of ac susceptibility as a function of the temperature in an ac field of 10 Oe of $Cu_{1.5}Mn_{1.5}O_4$ compound. The curve at each frequency suggests a clear peak at a specific temperature T_f, which is usually taken as the freezing temperature. The magnetic susceptibility $\chi'(T)$ presents a clear correlation with the frequency, which is accompanied by a decrease in the intensity of the peak and a shift towards high temperatures as the frequency increases. Such behavior of (χ') is a typical feature of the spin glass, cluster glass and super paramagnetic systems[51] caused by the intra-particle surface spin disorder or by strong magnetostatic interparticle interactions.[41,52]

We first calculated the phenomenological parameter C (Mydosh parameter), representing the relative shift of the peak position with respect to the frequency, being a new indicator to

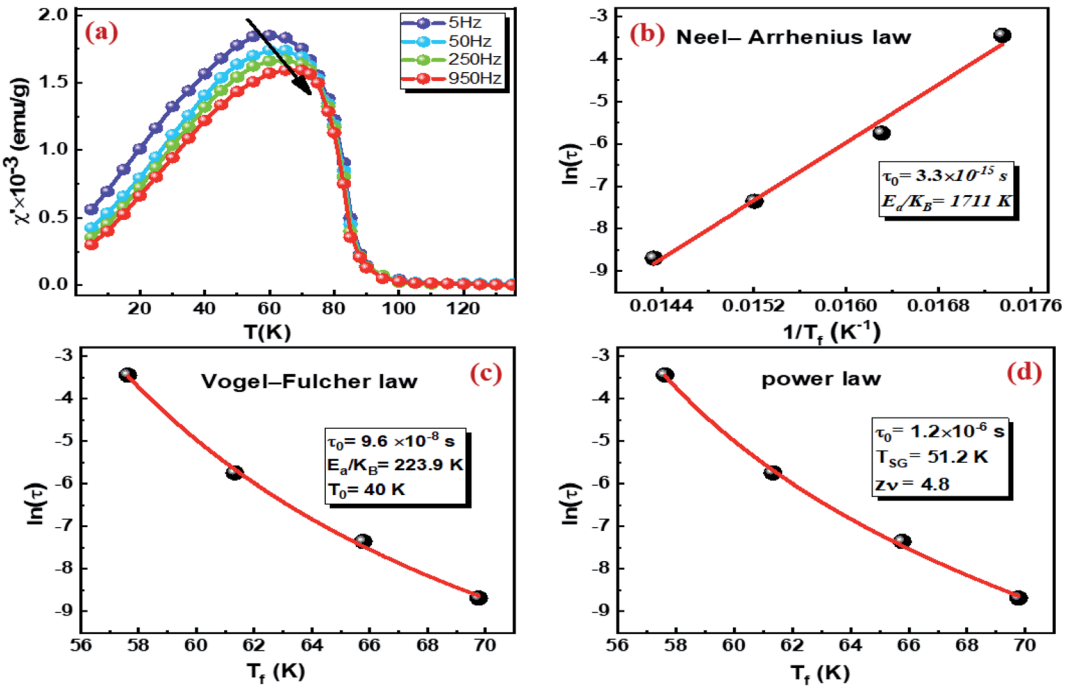

Fig. 2 Temperature dependence of magnetic susceptibility (χ') at different frequencies with an a.c. field of 10 Oe (a). The best fit of the relaxation times (τ) to the Neel–Arrhenius law (b) the Vogel–Fulcher law (c) and the power law (d) for the nanoparticles $Cu_{1.5}Mn_{1.5}O_4$.

distinguish the observed spin dynamic process[53] as per the following equation:

$$C = \frac{\Delta T_f}{T_f \Delta(\log_{10} f)} \quad (5)$$

whereby ΔT_f is the shift of the freezing temperature (T_f) at frequency f.

Generally, for spin glass and interacting particle systems C is located between 0.005 and 0.08,[54] for clustered glass, C is about 0.03–0.08,[54] for non-interacting superparamagnetism (SPM) C is between 0.1–0.13.[54] In the present case, it is found that C is equal to 0.08, which supports spin-glass and/or cluster glass freezing. Hence, the superparamagnetism is blocked.

In order to verify the interaction between clusters and their influence on the fluctuation dynamics, different phenomenological models such as Neel–Arrhenius, Vogel–Fulcher and power law are examined. For non-interacting isolated SPM compound, we try to fit the experimental data of the relaxation time (τ) *vs.* freezing temperature (T_f) by the Néel–Arrhenius law without any critical behavior:[55]

$$\tau = \tau_0 \exp\left(\frac{E_a}{K_B T_f}\right) \quad (6)$$

where τ_0 is the characteristic time of the system, E_a is the activation energy required to overcome the barrier of the reversal of the magnetization, K_B is the Boltzmann's constant and T_f the freezing temperature. For SPM relaxation, τ_0 depends on the gyromagnetic precession time, usually in the range of $\sim 10^{-10}$ to 10^{-13} s. As indicated in Fig. 2b, the best fit of our data gives $\tau_0 = 3.3 \times 10^{-15}$ s $\ll 10^{-13}$, excluding as such the possibility of the SPM property of particles. The value of E_a/K_B obtained from the best fit of $Cu_{1.5}Mn_{1.5}O_4$ sample is equal to 1711.1 K.

Accordingly, the relaxation behavior in the $Cu_{1.5}Mn_{1.5}O_4$ compound is described either by spin glass or cluster glass. The relaxation behavior in $Cu_{1.5}Mn_{1.5}O_4$ compound is described either by spin glass (SG) or by cluster glass (medium interaction). To further distinguish the state of relaxation behavior of copper manganite sample, we used Vogel–Fulcher's law, with an additional term T_0 to deal with the interaction between clusters:[55]

$$\tau = \tau_0 \exp\left(\frac{E_a}{K_B (T_f - T_0)}\right) \quad (7)$$

whereby T_0 is the characteristic SG transition temperature, which explains the interaction between particles, and its value is between zero and the freezing temperature T_f. The parameters τ_0, E_a/K_B and T_0 obtained from the best fit of the data in Fig. 2c with eqn (7) are 9.6×10^{-8} s, 223.9 K and 40 K, respectively. Theoretically, τ_0 is between 10^{-9} and 10^{-11} s for non-interacting particles and 10^{-6} and 10^{-10} for cluster glass while for SG system τ_0 is within 10^{-11} to 10^{-13} s.[54] The value of $\tau_0 = 9.6 \times 10^{-8}$ s deduced from the adjustment confirms the cluster glass behavior.

On the other hand, the parameter proposed by Tholence δ_{Th} related to the Vogel–Fulcher method is generally used to identify the type of spin interaction:[55]

$$\delta_{Th} = \frac{T_f - T_0}{T_f} \quad (8)$$

Table 2 The δ_{Th} values obtained at different frequencies

f (Hz)	δ_{Th}
5	0.31
50	0.34
250	0.39
950	0.42

Generally, δ_{Th} is equal to 1 for the non-interacting particles (SPM). For the cluster glass system (weak interaction regime), the value of δ_{Th} must range between 0.3–0.6, while for spin-glass (SG) system (the medium to strong interaction regime), it's within 0.07–0.3.[56] The δ_{Th} values obtained at different frequencies (see Table 2), characterize a weak interaction mechanism between the magnetic entities. This implies the existence of cluster glass state in the $Cu_{1.5}Mn_{1.5}O_4$ sample.

Finally, the critical spin dynamics, described by the conventional power law model, was exploited to eliminate the possibility of the spin glass behavior in the particle:[55]

$$\tau = \tau_0\left(\frac{T_f}{T_{SG}} - 1\right)^{-z\nu} \quad (9)$$

where τ_0 is the characteristic time of the system, T_f the freezing temperature, T_{SG} is the critical glass temperature and $z\nu$ a critical exponent. The parameters τ_0, T_{SG} and $z\nu$ obtained from the fitting of experimental data (Fig. 2d) are 1.2×10^{-6} s, 51.2 K and 4.8, respectively. Souletie and Tholence reported, that for the spin-glass state system, τ_0 is between 10^{-10} to 10^{-13} s and $z\nu$ within 4 and 13.[57] The τ_0 values obtained from Vogel–Fulcher and power law confirm that the spin-glass properties do not originate from atoms, but are related to clusters of atoms and therefore we would recognize it as a cluster glass. These values are significant and comparable to the results reported for some cluster glass systems.[54] The above results show that $Cu_{1.5}Mn_{1.5}O_4$ compound exhibit cluster glass behavior at 40 K due to the interaction between surface spins and ordered core spins, indicating that this material could be a promising candidate for some applications such as hypothermia and contrast enhancement agents for magnetic resonance imaging (MRI).[58,59]

Fig. 3a presents isothermal magnetization curves recorded in the temperature range of 22–122 K in a magnetic field up to 5 T with temperature step 3 K. Below T_C, the magnetization M increases rapidly and reaches saturation for low applied field values (0.5 T). This rapid increase corresponds to a rapid rearrangement of the Weiss domains in the direction of the applied magnetic field. This confirms a characteristic of FIM materials.[34] Above T_C, a decrease of $M(\mu_0 H)$ is observed with an almost linear behavior, which is typical for PM materials.[34] Fig. 3b demonstrates the Arrott plots (H/M *vs.* M^2) for $Cu_{1.5}Mn_{1.5}O_4$ which are derived from the isothermal magnetizations. All curves in the Arrott graph show nonlinear behaviors, even in the high field region, indicating that critical behavior of $Cu_{1.5}Mn_{1.5}O_4$ cannot be described by the conventional Stoner model. All the H/M *vs.* M^2 curves show a positive slope. According to the criteria proposed by Banerjee,[60] it suggests the occurrence of second-order magnetic transition. However, the non-linearity of the H/M *vs.* M^2 indicates that the classical Arrott graph is invalid for $Cu_{1.5}Mn_{1.5}O_4$.

3.3 Magnetocaloric properties

In order to better elucidate the utility of our compound in magnetic refrigeration systems, the magnetic entropy change (ΔS_M) induced indirectly from the isothermal magnetization curves, can be calculated using the approximated Maxwell equation.[61] Therefore, the variation of the magnetic entropy can be computed numerically based on this equation:[62]

$$\Delta S_M(T, \mu_0 H_{max}) = \sum_i \frac{M_{i+1}(T_{i+1}, \mu_0 H_{max}) - M_i(T_i, \mu_0 H_{max})}{T_{i+1} - T_i} \Delta \mu_0 H_{max} \quad (10)$$

where, M_i, M_{i+1} are experimentally magnetization measured under the application of the field $\mu_0 H$ of the temperatures respectively T_i and T_{i+1}.

Fig. 4a illustrates the temperature dependence of the magnetic entropy change ($-\Delta S_M(T)$) under different magnetic fields for $Cu_{1.5}Mn_{1.5}O_4$ compound. The magnitude of $-\Delta S_M$ increases as applied magnetic field increases and reached a maximum of 1.54, 2.52, 3.3, 3.97 and 4.58 J kg^{-1} K^{-1},

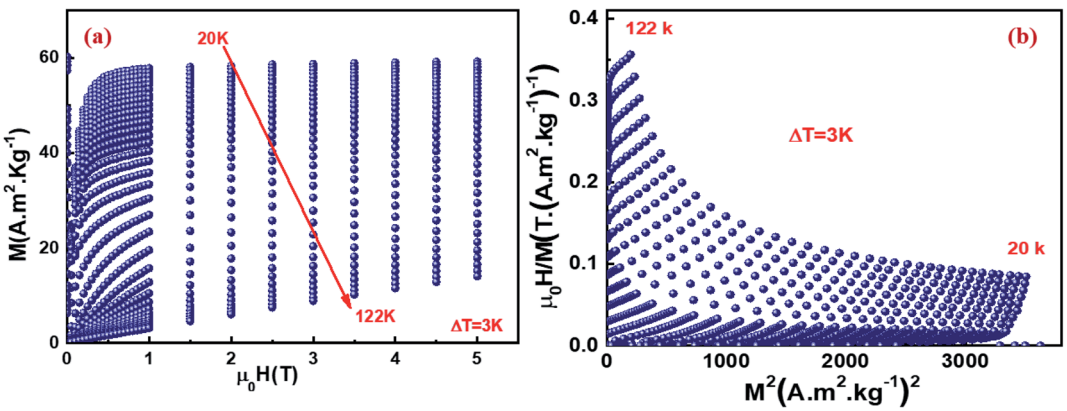

Fig. 3 Isothermal magnetization curves for $Cu_{1.5}Mn_{1.5}O_4$ nanoparticles measured at different temperatures around T_C. (a). Arrott plot ($\mu_0 H/M$ *vs.* M^2) isotherms (b).

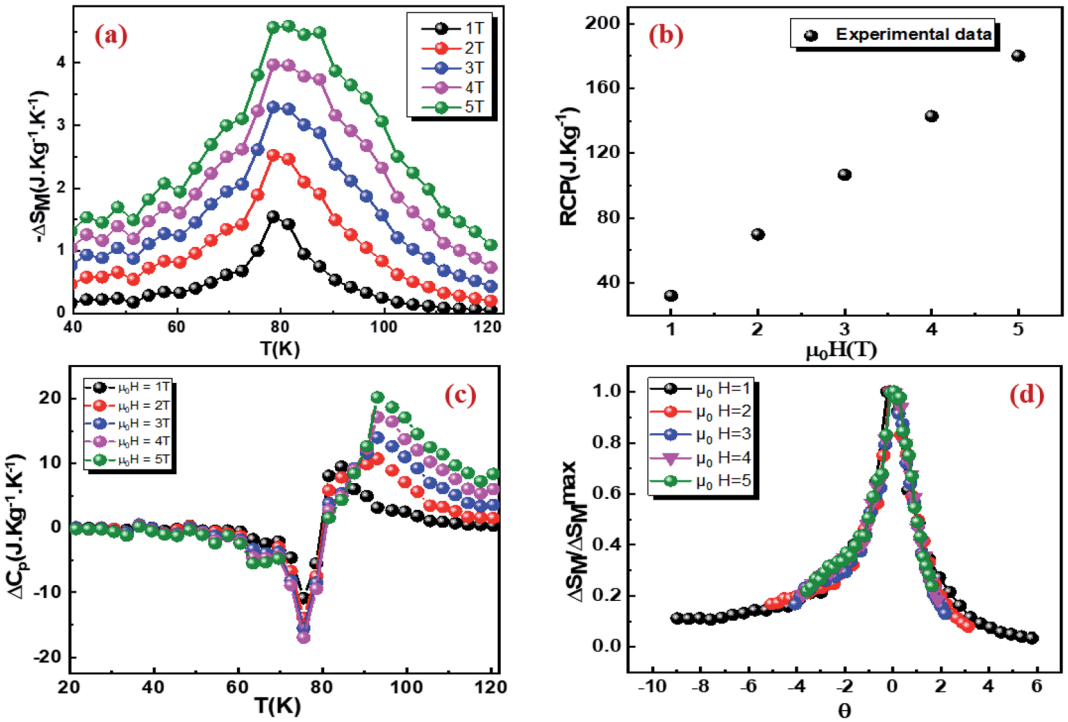

Fig. 4 Temperature dependence of the magnetic entropy change ($-\Delta S_M$) under applied fields ranging from 1 to 5 T (a). Variation of (RCP) as a function of ($\mu_0 H$) (b). Specific heat change (ΔC_p) as a function of temperature at different applied magnetic fields (c) and normalized entropy change ($\Delta S_M/\Delta S_M^{max}$) as a function of rescaled temperature (θ) for $Cu_{1.5}Mn_{1.5}O_4$ nanoparticles (d).

distribute around the Curie temperature T_C, for an applied magnetic field of 1, 2, 3, 4 and 5 T, respectively. To evaluate the cooling efficiency of our sample in the magnetic refrigeration field, we should calculate the relative cooling power (RCP)[63] corresponding to the quantity of the heat transfer between the cold and hot sinks in the ideal refrigeration cycle, expressed as:

$$\mathrm{RCP} = -\Delta S_M^{max} \times \delta T_{FWHM} \quad (11)$$

whereby, ΔS_M^{max} is the maximum entropy change obtained at $T = T_C$ and δT_{FWHM} is a full width at half maximum.

The RCP dependence of temperature at under different applied magnetic fields is displayed in Fig. 4b. It should be noted that gadolinium (Gd) is the best material that can be used in magnetic refrigeration at room temperature.[64] The obtained values of ($-\Delta S_M^{max}$) and (RCP) for our compound $Cu_{1.5}Mn_{1.5}O_4$ are compared with the Gd as a reference and other magnetic spinel under 4 and 5 T presented in Table 3. The ($-\Delta S_M^{max}$) and (RCP) values correspond to about 48.21 and 44% of those observed in pure Gd at 5 T. It is worth noting that the (RCP) value is high.[34,65] Thus, our compound can be considered as active magnetic refrigerants.

Table 3 Comparison of ($-\Delta S_M^{max}$) and (RCP) values for our compound $Cu_{1.5}Mn_{1.5}O_4$ with several materials under 4 and 5 T

Material	$-\Delta S_M^{max}$ (J kg^{-1} K^{-1})	RCP (J kg^{-1})	Ref.
Magnetic field	4–5 T	4–5 T	
Gd	9.5	410	64
$Cu_{1.5}Mn_{1.5}O_4$	3.97–4.58	143–180.13	This work
$CuMn_2O_4$	2.24–2.75	40.2–50.13	34
$NiCeFeO_4$	0.35–0.43	52.5–70.4	65

Fig. 4c displays the predicted results of the specific heat change (ΔC_p) *versus* temperature under different field calculated by using the following formula:

$$\Delta C_p = T\left[\frac{\partial \Delta S_M}{\partial T}\right]_{\mu_0 H} \quad (12)$$

whereby, ΔS_M the magnetic entropy change and $\mu_0 H$ the applied magnetic field.

The (ΔC_p) presents a negative value below T_C and a positive one above T_C that can strongly modify the total specific heat, which affects the heating or cooling power of the magnetic refrigerator.[66]

To further investigate the order of the magnetic phase transition in the sample, Franco *et al.*[67] have suggested a phenomenological universal curve of the temperature dependence of the magnetic entropy ΔS_M measured for different fields. Their suggestion is based on the assumption that, in the case of a second-order phase transition, all curves of the variation of magnetic entropy measured under different applied magnetic fields should collapse into one single new universal curve. While, in the case of a first order phase transition, the scaled curves do not obey a universal behavior.[68] The construction of the phenomenological universal curve was performed by normalizing all the magnetic entropy change curves ΔS_M with respect to their peak ΔS_M^{max} ($\Delta S_M/\Delta S_M^{max}$) with

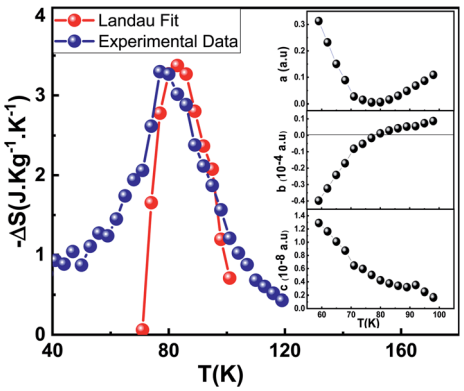

Fig. 5 Experimental and theoretical magnetic entropy changes for $Cu_{1.5}Mn_{1.5}O_4$ nanoparticles under 3 T applied magnetic field, the insets display the temperature dependence on Landau's coefficients $a(T)$, $b(T)$ and $c(T)$.

the redimensioning of the temperature axis using two additional reference temperatures in a different way below and above T_C as follows:[69]

$$\theta = \begin{cases} -(T - T_C)/(T_{r1} - T_C); & T \le T_C \\ (T - T_C)/(T_{r2} - T_C); & T > T_C \end{cases} \quad (13)$$

whereby, θ is the rescaled temperature, T_{r1} and T_{r2} are the temperature of the two reference points of each curve that, for the present study, T_{r1} and T_{r2} have been selected as temperatures corresponding to $\Delta S_M\,(T_{r1,2}) = (1/2)\Delta S_M^{max}$.

Fig. 4d unveils the universal curves of the magnetic entropy change of the $Cu_{1.5}Mn_{1.5}O_4$ compound measured for the applied fields ranging from 1 up to 5 T. It is evident that all the normalized entropy change curves are reduced to a single curve, verifying the second-order FIM-PM phase transition for our material and displaying, therefore, a good agreement between Banerjee criterion and the Franco approximation.

Concerning the theoretical modeling of the magnetocaloric effect (MCE), Amaral *et al.* suggested a model based on the Landau theory of phase transition that takes into account the interaction between electrons and the magnetoelastic coupling effects in manganites.[70,71] The magnetic energy $M(\mu_0 H)$ has been included in the expression of the Gibb's free energy.[72] Based on the equilibrium condition at the Curie temperature, the obtained relation between the magnetization and the applied field can be written as:

$$\frac{\mu_0 H}{M} = a(T) + b(T)M^2 + c(T)M^4 \quad (14)$$

Landau's parameters $a(T)$, $b(T)$ and $c(T)$ and their dependence on temperature determined from a polynomial fit of the experimental isothermal magnetizations ($\mu_0 H/M$ *vs.* M^2) as illustrated in the inset (Fig. 5). We can notice that $a(T)$ is always positive[70,73] with a minimum at the Curie temperature T_C corresponding to a maximum of the susceptibility, the sign of the Landau coefficient $b(T)$ indicates the order of magnetic phase transition and includes the magnetoelastic and elastic contributions, $b(T_C)$ can be negative, zero, or positive. If $b(T_C)$ is negative, the transition is a first order; otherwise, it is a second order. Therefore, the magnetic transition in our compound $Cu_{1.5}Mn_{1.5}O_4$ seems a second order. The magnetic entropy change is theoretically obtained by applying the differentiation of the free energy with respect to temperature, which has been given by the following equation:[74]

$$-\Delta S_M(\mu_0 H, T) = \left[\frac{\partial G}{\partial T}\right]_{\mu_0 H} = \frac{1}{2}a'(T)M^2 + \frac{1}{4}b'(T)M^4 + \frac{1}{6}c'(T)M^6 \quad (15)$$

where $a'(T)$, $b'(T)$ and $c'(T)$ are the temperature derivatives of the Landau coefficients.[63]

Fig. 5 exhibits a comparison between the magnetic entropy behavior obtained from the Maxwell relation integration of the experimental data from a magnetic field $\mu_0 H = 3$ T and that calculated using Landau's theory. The theoretical and experimental curve of our sample shows some difference, especially below T_C. Furthermore, the observed deviation of theoretically calculated ΔS from experimental results can be ascribed to magnetic disorder in the majority FIM phase. The existence of magnetic disorder inside the structure increases magnetization values for high-field values due to the unsaturated behavior of $M(\mu_0 H)$ isotherms, resulting in small shifts of Landau coefficients.[75] These shifts will certainly affect theoretical ΔS values below T_C. In our case, we are mainly interested in the use of the Landau theory to determine the maximum value of the exchange magnetic entropy and of T_C, to compare them with the experimental. A good agreement is found between the experimental magnetic entropy change and the theoretical one in the vicinity of T_C, which proves that both electron interaction and magnetoelastic coupling can account for the MCE properties,[70,76] and determine the phase transition of this sample without taking into consideration either the Jahn–Teller distortion or exchange interaction.[60]

We determined the spontaneous magnetization (M_S) in our $Cu_{1.5}Mn_{1.5}O_4$ compound from the magnetic entropy ΔS_M:[77–79]

$$-\Delta S(M) = \frac{3}{2}\frac{K_B}{Ng^2\mu_B{}^2 J(J+1)}\left(M^2 + M_S{}^2\right) \quad (16)$$

whereby, N is the number of spins, K_B is the Boltzmann constant, J is the spin value and g is the Landé factor.

According to eqn (16), the plot of the isotherms ($-\Delta S_M$) *vs.* M^2 is depicted in Fig. 6a. All the experimental data exhibit a linear variation. By fitting the ($-\Delta S_M$) *vs.* M^2 data for $T < T_C$, the value of M_S can be calculated through the intersection of the straight lines with the M^2 axis. For $T > T_C$, the ($-\Delta S_M$) *vs.* M^2 curves start at a null M value. On the other side, the linear fit applied in the linear regions of (H/M) *vs.* M^2 allows us to determine the values of M_S *vs.* T in Fig. 6b. Fig. 6c displays the spontaneous magnetization (M_S) as a function of temperature. We notice that the temperature decreases as, the spontaneous magnetization increases, indicating that the system is approaching a spin ordering state at lower temperature. A good agreement was noticed in the behavior of M_S *vs.* T estimated from ($-\Delta S_M$) *vs.* M^2 curves (blue symbols) and the $\mu_0 H/M$ *vs.* M^2 Arrott curves (red symbols). This confirms the validity of the

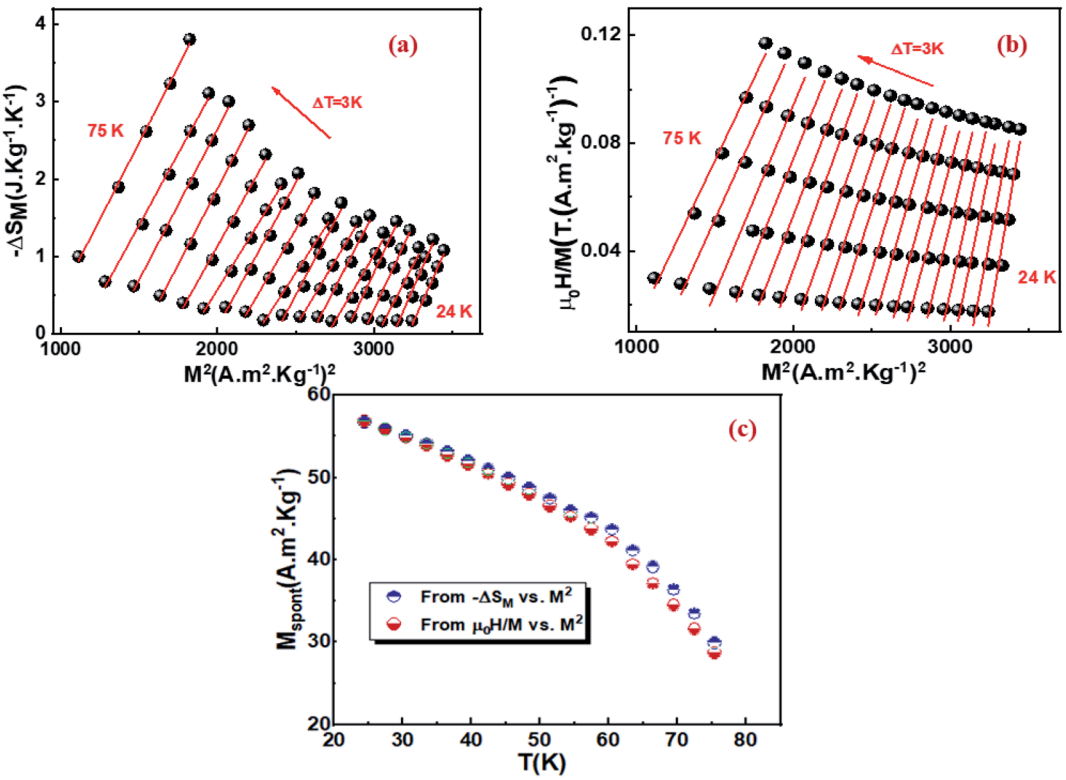

Fig. 6 Isothermal ($-\Delta S_M$ *vs.* M^2) curves (a). Arrott plots ($\mu_0 H/M$ *vs.* M^2) (b). Spontaneous magnetization of $Cu_{1.5}Mn_{1.5}O_4$ nanoparticle, deduced from the extrapolation of the isothermal ($-\Delta S_M$ *vs.* M^2) curves and from the Arrott plots ($\mu_0 H/M$ *vs.* M^2) (c).

change in magnetic entropy to determine the spontaneous magnetization values $M_S(T)$ of the $Cu_{1.5}Mn_{1.5}O_4$ compound.

3.4 Critical behavior study

In accordance with the scaling hypothesis, a second-order magnetic material, near the Curie temperature T_C, is characterized by a set of critical exponent β, γ, and δ,[80] for instance, are associated with the spontaneous magnetization M_S below T_C, the magnetic susceptibility χ_0^{-1} above T_C and the critical magnetization isotherm at $M(H, T = T_C)$, respectively. The magnetization measurements are linked to these exponents as per the following asymptotic relations:[81,82]

$$M_S(T < T_C, \mu_0 H \to 0) = M_0|\varepsilon|^{\beta} \quad (17)$$

$$\chi_0^{-1}(T > T_C, \mu_0 H \to 0) = \frac{h_0}{M_0}|\varepsilon|^{\gamma} \quad (18)$$

$$M(T = T_C, \mu_0 H) = D(\mu_0 H)^{\frac{1}{\delta}} \quad (19)$$

whereby, $\varepsilon = (T - T_C)/T_C$ is the reduced temperature, M_S the spontaneous magnetization, χ_0^{-1} the initial susceptibility, and M_0, $\frac{h_0}{M_0}$ and D refer to the critical amplitudes.

In order to determine the Curie temperature T_C as well as the critical exponents, various methods were used, such as the modified Arrott plot method "MAP", the Kouvel–Fisher method "KF" and the critical isotherm analysis "CIA". In the present study, to determine the most adequate model leading to correct exponents and a set of reasonably good parallel straight lines. Data analysis was carried out using a modified Arrott-plot "MAP" expression.[83]

Fig. 7a–d demonstrates the modified Arrott plots (MAP) at different temperatures of the $Cu_{1.5}Mn_{1.5}O_4$ compound obtained through diverse models: the mean-field model ($\beta = 0.5$, $\gamma = 1$ and $\delta = 3$), the 3D Heisenberg model ($\beta = 0.365$, $\gamma = 1.336$ and $\delta = 4.80$), the 3D Ising model ($\beta = 0.325$, $\gamma = 1.240$ and $\delta = 4.82$) and the tri-critical mean field model ($\beta = 0.25$, $\gamma = 1$ and $\delta = 5$). We observe at high fields, quasi-straight and nearly parallel lines, that seems difficult to differentiate the satisfactory model explaining the magnetic behavior for our compound.

In that case we calculate the relative slope (RS), as a new indicator to identify the best model, from the following equation:

$$\mathrm{RS} = \frac{S(T)}{S(T_C)} \quad (20)$$

whereby (T) and $S(T_C)$ is the MAP curve slope around and at T_C, respectively.

The most satisfactory model is that which have an RS close to 1 (unit).[82]

Fig. 8 showcase the RS *versus* T curve of our compound for the four models. It can be observed that the 3D-Ising model is the most suitable model to describe the magnetic interactions inside $Cu_{1.5}Mn_{1.5}O_4$ compound.

According to the "MAP", the linear extrapolation of the curves at high field region of the isotherm makes to determine

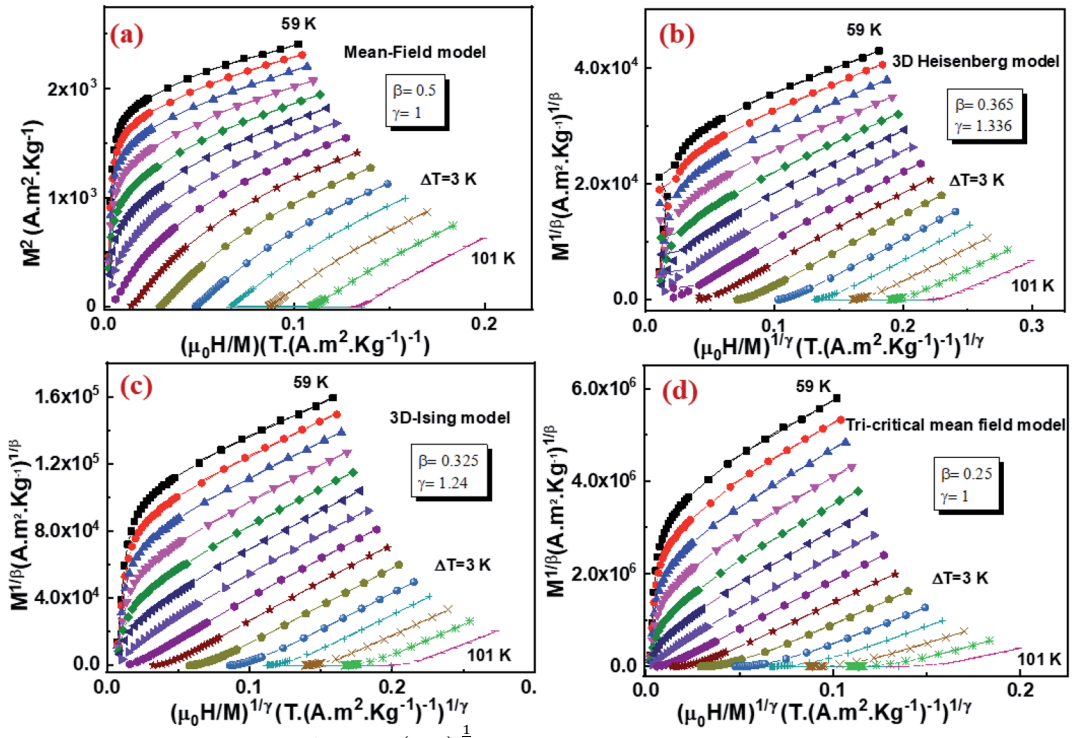

Fig. 7 Modified Arrott plots isotherms (MAP) $M^{\frac{1}{\beta}}$ *versus* $\left(\frac{\mu_0 H}{M}\right)^{\frac{1}{\gamma}}$ for $Cu_{1.5}Mn_{1.5}O_4$ nanoparticles, with mean-field model ($\beta = 0.5$, $\gamma = 1$) (a), 3D Heisenberg model ($\beta = 0.365$, $\gamma = 1.336$) (b), 3D Ising model ($\beta = 0.325$, $\gamma = 1.240$) (c) and tri-critical mean field model ($\beta = 0.25$, $\gamma = 1$) (d).

the values of the spontaneous magnetization (M_S) and the inverse of the initial paramagnetic susceptibility ($1/\chi$). The variations of $M_S(T)$ and $\chi^{-1}(T)$ *versus* temperature are reported in Fig. 9a. The fitting of these plots as per eqn (17) and (18) gives us the values of the β and γ exponents as well as the value of T_C (for details on the fits values, please see Table 3). We notice that the obtained critical exponents are very nearby to those associated with the best models obtained from RS curves.

A second method was exploited for more accurate determination of the critical exponent and T_C value, known as Kouvel–Fisher "KF" method.[84] This procedure is based on the following expressions:

$$M_S(T)\left(\frac{dM_S(T)}{dT}\right)^{-1} = \frac{T - T_C}{\beta} \quad (21)$$

$$\chi_0^{-1}(T)\left(\frac{d\chi_0^{-1}(T)}{dT}\right)^{-1} = \frac{T - T_C}{\gamma} \quad (22)$$

Referring to eqn (21) and (22), we have plotted $M_S(T)\left(\frac{dM_S(T)}{dT}\right)^{-1}$ and $\chi_0^{-1}(T)\left(\frac{d\chi_0^{-1}(T)}{dT}\right)^{-1}$ *versus* temperature. The plots follow a linear behavior with the slopes $1/\beta$ and $1/\gamma$, respectively, and the intersections on the temperature axis give the values of T_C.[84]

The KF plot has been presented in Fig. 9b. The values of the critical exponents as well as the Curie temperature are gathered in Table 4. We can notice that the obtained values of β and γ exponents as well as that of T_C, calculated using both procedures, are consistent with each other. This suggests that the Arrott–Noakes and KF method are both feasible and effective to study the critical properties.

Fig. 10 presents the critical isotherm curve $M(H)$ at $T_C = 80$ K. Using eqn (19), we can determine the third critical exponent δ from a linear adjustment of the $M(H)$ at high field plotted on a log scale at the Curie temperature (see the inset of Fig. 10).

The exponent δ can be also calculated from Widom scaling law given by:[85]

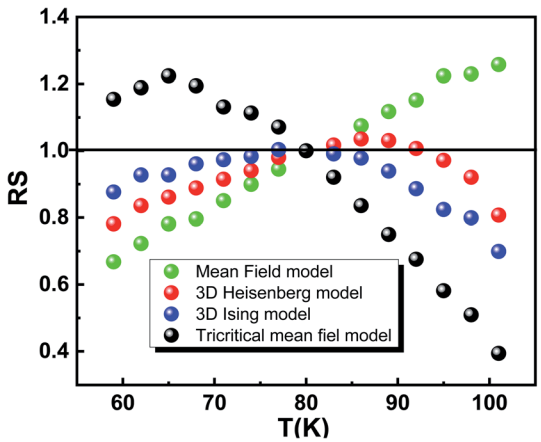

Fig. 8 Relative slope (RS) as a function of temperature for $Cu_{1.5}Mn_{1.5}O_4$ nanoparticles.

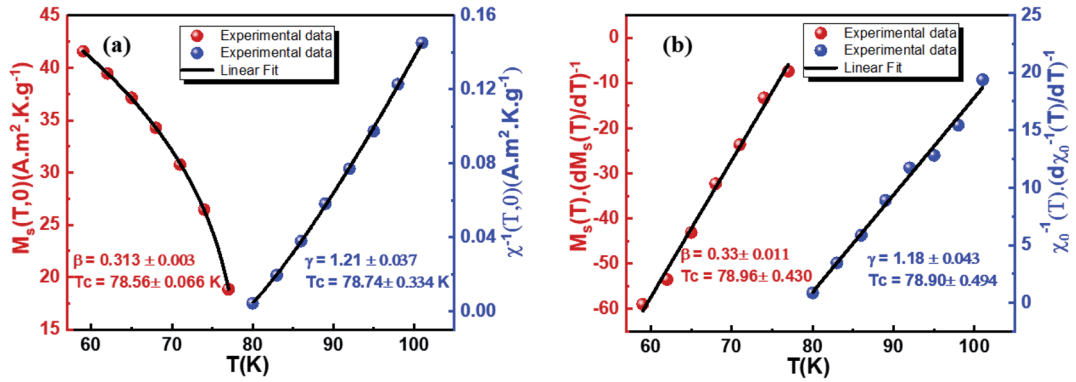

Fig. 9 Temperature dependence of spontaneous magnetization $M_S(T)$ and inverse initial susceptibility $\chi_0^{-1}(T)$ along with fitting curves based on the power laws for $Cu_{1.5}Mn_{1.5}O_4$ material (a). Kouvel–Fisher (KF) plot for the spontaneous magnetization $M_S(T)$ and the inverse susceptibility $\chi_0^{-1}(T)$, the solid lines are the linear fits of the data (b).

Table 4 Comparison of critical exponents of $Cu_{1.5}Mn_{1.5}O_4$ nanoparticles with the different theoretical models[a]

Model/sample	Technique	T_C (K)	β	γ	δ	Ref.
Mean field model	Theory		0.5	1	3	31
3D Heisenberg model	Theory		0.365	1.336	4.80	31
3D Ising model	Theory		0.325	1.240	4.82	31
Tri-critical mean field model	Theory		0.25	1	5	31
$Cu_{1.5}Mn_{1.5}O_4$	MAP	78.65 ± 0.4	0.313 ± 0.003	1.21 ± 0.037		This work
	KF	78.93 ± 0.462	0.33 ± 0.011	1.18 ± 0.043		This work
	CIA(exp.)				4.54 ± 0.002	This work
	CIA(cal.)				4.86	This work

[a] CI – critical isotherm, exp. – experimental, cal. – calculated and MAP – modified Arrott plots.

$$\delta = 1 + \frac{\gamma}{\beta} \tag{23}$$

Using this expression, the δ value is 4.86. This value is comparable to that obtained by the magnetic isotherms at T_C. The obtained values are summarized in Table 3. Consequently, these results ensure the reliability of the obtained β and γ values.

In order to test the reliability of the obtained critical exponent values, we have used the scaling hypothesis, assuming that both magnetization and internal magnetic field should obey the universal scaling law established by the following expression:[86]

$$M(\mu_0 H, \varepsilon) = |\varepsilon|^{\beta} f_{\pm}\left(\frac{\mu_0 H}{|\varepsilon|^{\beta+\gamma}}\right) \tag{24}$$

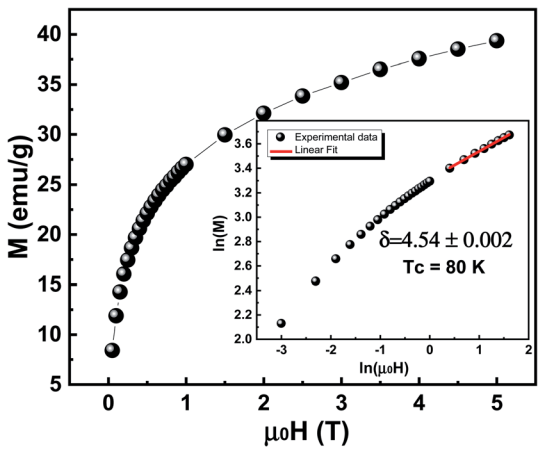

Fig. 10 Critical isotherms of (M *vs.* $\mu_0 H$) for $Cu_{1.5}Mn_{1.5}O_4$ nanoparticles. The inset displays the same curve on log–log scale.

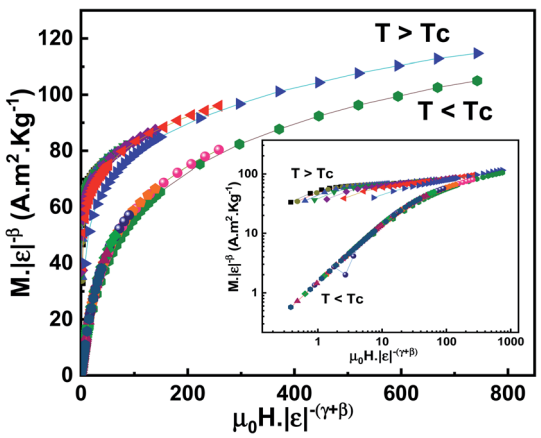

Fig. 11 Scaling plots indicating two universal curves below and above T_C for $Cu_{1.5}Mn_{1.5}O_4$ nanoparticles. The inset presents the same curve on a log–log scale.

where, f_+ for $T > T_C$ and f_- for $T < T_C$ are regular analytic functions.

We have plotted in Fig. 11 the evolution of $M|\varepsilon|^{-\beta}$ as a function of $\mu_0 H|\varepsilon|^{-(\beta+\gamma)}$ for the temperature range around T_C, using values of β, γ and T_C deduced from the "KF" method. By applying the logarithmic scale (in the inset of Fig. 11), we have carried out two independent branches, with the first one for temperature values below T_C and the second one for temperature values above T_C. As a result, these two universal curves confirm the agreement of the scaling hypothesis, suggesting the suitability of the obtained values of the critical exponents defining our model. The latter explains the magnetic interactions in compound.

4. Conclusion

In summary, the present research study examined the spin dynamics, the magnetic properties, the magnetocaloric effect and the critical behaviour near the magnetic phase transition temperature of $Cu_{1.5}Mn_{1.5}O_4$ compound. The frequency-dependent ac susceptibility (χ') data fitted with various phenomenological models such as the Neel–Arrhenius, Vogel–Fulcher and power law, suggests that the cluster glass state is formed in $Cu_{1.5}Mn_{1.5}O_4$ sample. The magnetic measurements display a second order paramagnetic (PM)/ferrimagnetic (FIM) phase transition at Curie temperature. We have as well investigated the magnetocaloric effect MCE using Maxwell relation and Landau theory for $Cu_{1.5}Mn_{1.5}O_4$. A good agreement was found between the experimental and theoretical calculations of $(-\Delta S)$ values of a magnetic field of 5 T, which reveals the importance of magnetoelastic coupling and electron interaction in the MCE properties of manganite systems. The relative cooling power (RCP) was predicted, which indicates that our material could be a good candidate for certain applications, including but not limited to refrigeration application. The magnetic entropy curves are found to follow the universal law, confirming the second-order ferrimagnetic (FIM) to paramagnetic (PM) phase transition at T_C for our material. Therefore, a good agreement has been shown between Banerjee criterion and the Franco approximation. The spontaneous magnetization values estimated from the magnetic entropy change ($(-\Delta S_M)$ *vs.* M^2) are in excellent agreement with those determined from the classical extrapolation of Arrott curves (H/M *vs.* M^2). By analyzing the isothermal magnetization around the Curie temperature T_C and using several techniques such as modified Arrott plot (MAP), Kouvel–Fisher (KF) method and critical isotherm analysis (CIA), the values of β, γ, δ and T_C are estimated.

The obtained results are coherent with the 3D-Ising model for $Cu_{1.5}Mn_{1.5}O_4$ compound. In addition the reliability of the critical exponent values was confirmed by Widom law, as well as the scaling hypothesis.

Conflicts of interest

The authors declare that they have no known competing financial interests or personal relationships that could have appeared to influence the work reported in this paper.

Acknowledgements

This work is supported by: The authors extend their appreciation to the Deputyship for Research & Innovation, Ministry of Education in Saudi Arabia for funding this work through the project number "375213500". The authors would like to extend their sincere appreciation to the central laboratory at Jouf University for supporting this study. The Tunisian National Ministry of Higher Education, Scientific Research and Technology.

References

1 P. N. Lisboa-Filho, M. Bahout, P. Barahona, C. Moure and O. Peña, *J. Phys. Chem. Solids*, 2005, **66**, 1206–1212.
2 G. Pilania, V. Kocevski, J. A. Valdez, C. R. Kreller and B. P. Uberuaga, *Commun. Mater.*, 2020, **1**, 84.
3 J. L. Dormann and M. Nogues, *J. Phys. Condens. Matter*, 1990, **2**, 1223.
4 T. Tsutaoka, *J. Appl. Phys.*, 2003, **93**, 2789–2796.
5 J. Massoudi, M. Smari, K. Nouri, E. Dhahri, K. Khirouni, S. Bertaina and L. Bessais, *RSC Adv.*, 2020, **10**, 34556–34580.
6 A. Bougoffa, J. Massoudi, M. Smari, E. Dhahri, K. Khirouni and L. Bessais, *J. Mater. Sci.: Mater. Electron.*, 2019, **30**, 21018–21031.
7 R. Peelamedu, C. Grimes, D. Agrawal, R. Roy and P. Yadoji, *J. Mater. Res.*, 2003, **18**, 2292–2295.
8 A. K. M. Akther Hossain, M. Seki, T. Kawai and H. Tabata, *J. Appl. Phys.*, 2004, **96**, 1273–1275.
9 S. Nayak, S. Thota, D. C. Joshi, M. Krautz, A. Waske, A. Behler, J. Eckert, T. Sarkar, M. S. Andersson and R. Mathieu, *Phys. Rev. B*, 2015, **92**, 214434.
10 W. Yang, X. Kan, X. Liu, Z. Wang, Z. Chen, Z. Wang, R. Zhu and M. Shezad, *Ceram. Int.*, 2019, **45**, 23328–23332.
11 Y. Moritomo, Y. Tomioka, A. Asamitsu, Y. Tokura and Y. Matsui, *Phys. Rev. B: Condens. Matter Mater. Phys.*, 1995, **51**, 3297.
12 J. A. Mydosh, *J. Magn. Magn. Mater.*, 1996, **157**, 606–610.
13 S. Karmakar, S. Taran, E. Bose, B. K. Chaudhuri, C. P. Sun, C. L. Huang and H. D. Yang, *Phys. Rev. B: Condens. Matter Mater. Phys.*, 2008, **77**, 144409.
14 S. Kirkpatrick and D. Sherrington, *Phys. Rev. B: Condens. Matter Mater. Phys.*, 1978, **17**, 4384.
15 R. D. McMichael, R. D. Shull, L. J. Swartzendruber, L. H. Bennett and R. E. Watson, *J. Magn. Magn. Mater.*, 1992, **111**, 29–33.
16 M. Zborowski, in *Physics of Magnetic Cell Sorting Scientific and Clinical Applications of Magnetic Carriers*, ed. M. Zborowski, Plenum, New York, 1997.
17 D. G. Mitchell, *J. Magn. Reson. Imaging*, 1997, **7**, 1–4.
18 K. Raj, B. Moskowitz and R. Casciari, *J. Magn. Magn. Mater.*, 1995, **149**, 174–180.
19 M. H. Kryder, *MRS Bull.*, 1996, **21**, 17–22.
20 V. V. Gridin, G. R. Hearne and J. M. Honig, *Phys. Rev. B: Condens. Matter Mater. Phys.*, 1996, **53**, 15518.
21 J.-M. Li, A. C. H. Huan, L. Wang, Y.-W. Du and D. Feng, *Phys. Rev. B: Condens. Matter Mater. Phys.*, 2000, **61**, 6876.

22 R. H. Kodama, A. E. Berkowitz, E. J. McNiff, Jr and S. Foner, *Phys. Rev. Lett.*, 1996, **77**, 394.
23 M. F. Jönsson, *Phys. Rev. B: Condens. Matter Mater. Phys.*, 2000, **61**, 1261.
24 D. Peddis, D. Rinaldi, G. Ennas, A. Scano, E. Agostinelli and D. Fiorani, *Phys. Chem. Chem. Phys.*, 2012, **14**, 3162–3169.
25 C. Tien, C. H. Feng, C. S. Wur and J. J. Lu, *Phys. Rev. B: Condens. Matter Mater. Phys.*, 2000, **61**, 12151.
26 J. A. Mydosh, *Spin glasses: an experimental introduction*, Taylor and Francis, 1993.
27 H. Szymczak, M. Baran, G.-J. Babonas, R. Diduszko, J. Fink-Finowicki and R. Szymczak, *J. Magn. Magn. Mater.*, 2005, **285**, 386–394.
28 K. Anil and P. A. Joy, *J. Phys. Condens. Matter*, 1998, **10**, L487–L493.
29 J. L. Alonso, L. A. Fernández, F. Guinea, V. Laliena and V. Martín-Mayor, *Nucl. Phys. B*, 2001, **596**, 587–610.
30 A. K. Pramanik and A. Banerjee, *Phys. Rev. B: Condens. Matter Mater. Phys.*, 2009, **79**, 214426.
31 H. E. Stanley, *Introduction to Phase Transitions and Critical Phenomena*, Oxford University Press, Oxford, 1971.
32 S. N. Kaul, *J. Magn. Magn. Mater.*, 1985, **53**, 5–53.
33 A. Waskowska, L. Gerward, J. S. Olsen, S. Steenstrup and E. Talik, *J. Phys. Condens. Matter*, 2001, **13**, 2549.
34 K. Vinod, A. T. Satya, N. R. Ravindran and A. Mani, *Mater. Res. Express*, 2018, **5**, 056104.
35 S. Mohanta, S. D. Kaushik and I. Naik, *Solid State Commun.*, 2019, **287**, 94–98.
36 H. Zhao, X. X. Zhou, L. Y. Pan, M. Wang, H. R. Chen and J. L. Shi, *RSC Adv.*, 2017, **7**, 20451–20459.
37 J. Quan, L. Mei, Z. Ma, J. Huang and D. Li, *RSC Adv.*, 2016, **6**, 55786–55791.
38 R. E. Vandenberghe, G. G. Robbrecht and V. A. M. Brabers, *Mater. Res. Bull.*, 1973, **8**, 571–579.
39 A. Hadded, J. Massoudi, E. Dhahri, K. Khirouni and B. F. O. Costa, *RSC Adv.*, 2020, **10**, 42542–42556.
40 A. Mabrouki, T. Mnasri, A. Bougoffa, A. Benali, E. Dhahri and M. A. Valente, *J. Alloys Compd.*, 2021, **860**, 157922.
41 J. A. Mydosh, *Spin glasses: an experimental introduction*, Taylor and Francis, 1993.
42 S. Mukherjee, R. Ranganathan, P. S. Anilkumar and P. A. Joy, *Phys. Rev. B: Condens. Matter Mater. Phys.*, 1996, **54**, 9267.
43 I. G. Deac, J. F. Mitchell and P. Schiffer, *Phys. Rev. B: Condens. Matter Mater. Phys.*, 2001, **63**, 172408.
44 S. G. Yang, T. Li, B. X. Gu, Y. W. Du, H. Y. Sung, S. T. Hung, C. Y. Wong and A. B. Pakhomov, *Appl. Phys. Lett.*, 2003, **83**, 3746–3748.
45 D. P. Shoemaker, J. Li and R. Seshadri, *J. Am. Chem. Soc.*, 2009, **131**, 11450–11457.
46 P. Patra, I. Naik, S. D. Kaushik, S. Mukherjee and S. Mohanta, 2020, arXiv preprint arXiv:2008.04571.
47 G. M. Al-Senani, O. H. Abd-Elkader and N. M. Deraz, *Appl*, 2021, **11**, 2034.
48 A. Tozri, J. Khelifi, E. Dhahri and E. K. Hlil, *Mater. Chem. Phys.*, 2015, **149**, 728–733.
49 M. Khlifi, M. Wali and E. Dhahri, *Phys. B*, 2014, **449**, 36–41.
50 S. Åsbrink, A. Waśkowska and E. Talik, *J. Phys. Chem. Solids*, 1999, **60**, 573–577.
51 D. Gangwar and C. Rath, *Phys. Chem. Chem. Phys.*, 2020, **22**, 14236–14245.
52 A. Tokarev, P. Agulhon, J. Long, F. Quignard, M. Robitzer, R. A. Ferreira, L. D. Carlos, J. Larionova, C. Guérin and Y. Guari, *J. Mater. Chem.*, 2012, **22**, 20232–20242.
53 M. K. Singh, W. Prellier, M. P. Singh, R. S. Katiyar and J. F. Scott, *Phys. Rev. B: Condens. Matter Mater. Phys.*, 2008, **77**, 144403.
54 D. Gangwar and C. Rath, *Phys. Chem. Chem. Phys.*, 2020, **22**, 14236–14245.
55 J. Massoudi, M. Smari, K. Khirouni, E. Dhahri and L. Bessais, *J. Magn. Magn. Mater.*, 2021, **528**, 167806.
56 D. M. Neacsa, G. Gruener, S. Hebert and J.-C. Soret, *J. Magn. Magn. Mater.*, 2017, **432**, 68–76.
57 J. Souletie and J. L. Tholence, *Phys. Rev. B: Condens. Matter Mater. Phys.*, 1985, **32**, 516.
58 S. Akhter, D. P. Paul, S. M. Hoque, M. A. Hakim, M. Hudl, R. Mathieu and P. Nordblad, *J. Magn. Magn. Mater.*, 2014, **367**, 75–80.
59 D. Soukup, S. Moise, E. Céspedes, J. Dobson and N. D. Telling, *ACS Nano*, 2015, **9**, 231–240.
60 K. Dey, A. Indra, S. Majumdar and S. Giri, *J. Magn. Magn. Mater.*, 2017, **435**, 15–20.
61 R. Skini, A. Omri, M. Khlifi, E. Dhahri and E. K. Hlil, *J. Magn. Magn. Mater.*, 2014, **364**, 5–10.
62 A. Mabrouki, A. Benali, T. Mnasri, E. Dhahri, M. A. Valente and M. Jemmali, *J. Mater. Sci.: Mater. Electron.*, 2020, **31**, 22749–22767.
63 M. Jeddi, H. Gharsallah, M. Bejar, M. Bekri, E. Dhahri and E. K. Hlil, *RSC Adv.*, 2018, **8**, 9430–9439.
64 V. K. Pecharsky and K. A. Gschneidner, Jr, *Phys. Rev. Lett.*, 1997, **78**, 4494–4497.
65 S. Bahhar, A. Boutahar, L. H. Omari, H. Lemziouka, E. K. Hlil and H. Bioud, *Solid State Commun.*, 2020, **322**, 114056.
66 M. Jeddi, H. Gharsallah, M. Bekri, E. Dhahri and E. K. Hlil, *J. Mater. Sci.: Mater. Electron.*, 2019, **30**, 14430–14444.
67 V. Franco, A. Conde, J. M. Romero-Enrique and J. S. Blázquez, *J. Phys. Condens. Matter*, 2008, **20**, 285207.
68 C. M. Bonilla, J. Herrero-Albillos, F. Bartolomé, L. M. García, M. Parra-Borderías and V. Franco, *Phys. Rev. B: Condens. Matter Mater. Phys.*, 2010, **81**, 224424.
69 R. Tlili, A. Omri, M. Bejar, E. Dhahri and E. K. Hlil, *Ceram. Int.*, 2015, **41**, 10654–10658.
70 V. S. Amaral and J. S. Amaral, *J. Magn. Magn. Mater.*, 2004, **272**, 2104–2105.
71 J. S. Amaral, M. S. Reis, V. S. Amaral, T. M. Mendonca, J. P. Araujo and M. A. Sa, *J. Magn. Magn. Mater.*, 2005, **290**, 686.
72 J. S. Amaral and V. S. Amaral, *J. Magn. Magn. Mater.*, 2010, **322**, 1552–1557.
73 J. Inoue and M. Shimizu, *Phys. Lett. A*, 1982, **90**, 85–88.
74 M. S. Anwar, S. Kumar, F. Ahmed, N. Arshi, G. W. Kim and B. H. Koo, *J. Korean Phys. Soc.*, 2012, **60**, 1587–1592.
75 W. Mabrouki, A. Krichene, N. C. Boudjada and W. Boujelben, *Appl. Phys. A*, 2020, **126**, 1–12.

76 S. Chandra, A. Biswas, M.-H. Phan and H. Srikanth, *J. Magn. Magn. Mater.*, 2015, **384**, 138–143.
77 A. M. Tishin and Y. I. Spichkin, *The magnetocaloric effect and its applications*, CRC Press, 2016.
78 X. Si, Y. Shen, X. Ma, S. Chen, J. Lin, J. Yang, T. Gao and Y. Liu, *Acta Mater.*, 2018, **143**, 306–317.
79 J. C. Debnath, A. M. Strydom, P. Shamba, J. L. Wang and S. X. Dou, *J. Appl. Phys.*, 2013, **113**, 233903.
80 H. E. Stanley, *Introduction to Phase Transitions and Critical Phenomena*, Oxford University Press, Oxford, 1971.
81 K. Huang, *Introduction to statistical physics*, New York, 1987, p. 263.
82 C. V. Mohan, M. Seeger, H. Kronmüller, P. Murugaraj and J. Maier, *J. Magn. Magn. Mater.*, 1998, **183**, 348–355.
83 A. Arrott and J. E. Noakes, *Phys. Rev. Lett.*, 1967, **19**, 786.
84 J. S. Kouvel and M. E. Fisher, *Phys. Rev.*, 1964, **136**, A1626.
85 N. Assoudi, I. Walha, K. Nouri, E. Dhahri and L. Bessais, *J. Alloys Compd.*, 2018, **753**, 282–291.
86 J. Yang and Y. P. Lee, *Appl. Phys. Lett.*, 2007, **91**, 142512.